HEFAT2014
10th International Conference on Heat Transfer, Fluid Mechanics and Thermodynamics
14 – 16 July 2014
Orlando, Florida

OPTIMIZATION OF MODEL WIND-TUNNEL CONTRACTION USING CFD

Ahmed D. E.[(1)] and Eljack E. M [(1,2)]
[(1)]Department of Mechanical Engineering, University of Khartoum,
Khartoum, P.O. Box 321, Sudan,
E-mail: daniaahmed@uofk.edu
[(2)]Aeronautical Engineering Department, King AbdulAziz University,
Jeddah, P. O. Box 80204, KSA,
E-mail: emeljack@uofk.edu , eljack@kau.edu.sa

ABSTRACT

Computational Fluid Dynamics is used as a tool for optimizing a model wind tunnel three-dimensional contraction. A sixth order polynomial profile is chosen with six conditions to determine the polynomial coefficients. The seventh condition is the location of the inflection point along the contraction axis. Five inflection points are chosen to give five different contractions. Numerical simulations for the five contractions are carried out, Reynolds number based on the free stream velocity and the test section height is 1.3×10^6. Boundary layer thickness, static pressure and secondary flow are considered as optimization parameters. Numerical results show that boundary layer thickness decreases, variation in wall normal velocity components at the test section inlet increases, and probability of flow separation increases as the inflection point moves towards the contraction outlet. Unlike recent numerical studies, numerical results of this work indicate that the optimum profile for the contraction is when the inflection point is located at the middle of the contraction, thus the sixth order polynomial reduces to a fifth order.

INTRODUCTION

Wind-tunnels represent a useful tool for investigating various flow phenomena. An advantage of using wind-tunnels is that experiments there can be performed under well controlled flow circumstances compared to experiments in the open environment.

For flow quality improvement, most important part in the wind-tunnel circuit is the contraction through which the flow passes before entering the test section. In the contraction the flow is accelerated rapidly, this results in a large stream wise strain that reduces mean flow variations and the larger the contraction ratio (CR), the larger the strain and thus reduction in static pressure.

The contraction has two main objectives; the first one is to increase the mean velocity of the flow, this in turn reduce the pressure losses in honeycombs and screens, as the flow moves through with lower speed. The second objective is to reduce both mean and fluctuating velocity variations to a smaller fraction of the mean velocity and consequently provide a low turbulence intensity flow at the test-section. The most important independent parameter for determining velocity variations is the contraction ratio (C_R), in this study $C_R = 9$.

The contraction can be divided into two parts; the first part has walls of concave shape and it is very important to elongate this part as much as possible to avoid wall boundary layer separation to occur here. The second part of the contraction has convex walls. Here, there is also a risk of separation close to the test section since there is a positive pressure gradient. It is easy to counteract a separation in this section by using some boundary layer tripping device such as tape with V-shaped roughness elements.

Traditionally, the design of wind tunnel contractions (three dimensional) has been based on two parts, the joining point location used to be the design optimisation parameter for a fixed length and contraction ratio. In this study, however, the location of inflection point along the contraction axis is used as an optimization parameter.

NOMENCLATURE

C_R	[-]	Contraction ratio
H_i	[m]	The contraction inlet height
H_o	[m]	The contraction outlet height
k	$[m^2/s^2]$	Turbulence kinetic energy (TKE)
L	[m]	The contraction length
$\tilde{p}$	$[N/m^2]$	Instantaneous pressure
P	$[N/m^2]$	Mean pressure
$\tilde{u}$	[m/s]	Instantaneous velocity component in x-direction
$\tilde{v}$	[m/s]	Instantaneous velocity component in y-direction
$\tilde{w}$	[m/s]	Instantaneous velocity component in z-direction
U	[m/s]	Mean velocity component in x-direction
V	[m/s]	Mean velocity component in y-direction
W	[m/s]	Mean velocity component in z-direction
x	[m]	Cartesian axis direction
y	[m]	Cartesian axis direction
z	[m]	Cartesian axis direction
Greek letters		
ε	[m]	Location of inflection point along contraction axis
ν	$[m^2/s]$	Kinematic viscosity
ρ	$[kg/m^3]$	Fluid density
ω	[1/s]	Energy dissipated per unit TKE

GEOMETRY

As a result of the geometrical symmetry of the contraction and test section, one quarter of both the contraction and the test section is considered in the simulation. The geometry specifications are as follows:

- The contraction inlet height is 0.75m.
- Contraction length 1.5m.
- Test section height 0.25m.
- Test section length 1.5m.

The main difference between the five contractions is the location of the inflection point at the profile of contraction. Figure 1 shows the computational geometry.

CONTRACTION PROFILES

Considering a sixth order polynomial equation for the contraction profile shape, shown in equation (1).

$$y = ax^6 + bx^5 + cx^4 + dx^3 + ex^2 + fx + g \quad (1)$$

Boundary conditions for determining the coefficients a, b, c, d, e, and f are:

1- At contraction inlet: x = 0 m and y =$H_i = 0.75\ m$.
2- At contraction exit: x =1.5 m and y =$H_o = 0.25\ m$.
3- The slope equals zero at the contraction inlet:
   x = 0 m, $\frac{dy}{dx} = 0$.
4- The slope equals zero at the contraction outlet:
   x = 1.5 m, $\frac{dy}{dx} = 0$.
5- The radius of curvature at the contraction inlet equals zero:
   x = 0 m, $\frac{d^2y}{dx^2} = 0$.
6- The radius of curvature at the contraction outlet equals zero:
   x = 1.5 m, $\frac{d^2y}{dx^2} = 0$
7- Inflection point ε; x= ε, $\frac{d^2y}{dx^2} = 0$, five locations for the inflection point are considered; at x=0.600, 0.657, 0.750, 0.825 and 0.900.

The coefficient for each inflection location is determined, and shown in table 1.

Table 1 Polynomial coefficients for each contraction profile, for all profiles e=0, f=0 and g=H_i.

ε	Profile	a	b	c	d
0.600	One	0.44	-2.37	4.44	-2.96
0.675	Two	0.18	-1.23	2.73	-2.11
0.750	Three	0.00	-0.40	1.48	-1.48
0.825	Four	-0.18	0.44	0.23	-0.86
0.900	Five	-0.44	1.58	-1.48	0.00

Figure 1 shows the different contraction profiles. The sixth order polynomial equation reduced to a fifth order one when the inflection point located at the middle of contraction length.

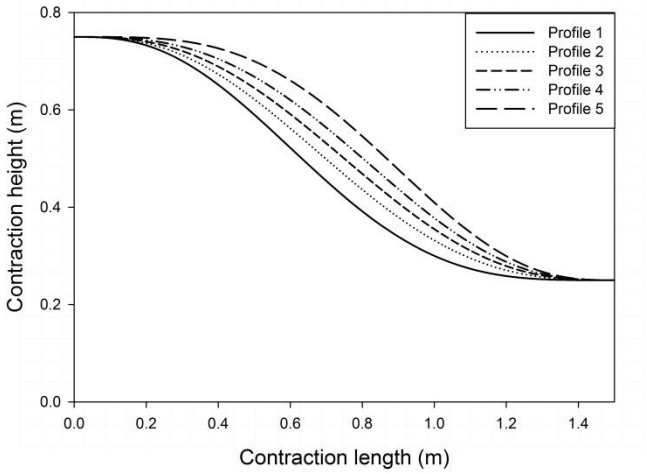

Figure 1 Contraction profiles

GOVERNING EQUATIONS

Fluid flow is governed by Navier-Stokes equations that, in Cartesian coordinates, can be written in tensor notations as follows:

$$\frac{\partial \tilde{u}_i}{\partial t} + \tilde{u}_j \frac{\partial \tilde{u}_i}{\partial x_j} = -\frac{1}{\rho}\frac{\partial \tilde{p}}{\partial x_i} + \nu \frac{\partial^2 \tilde{u}_i}{\partial {x_j}^2}$$

Direct solution of these equations numerically is very expensive, however, a cheap form of these equation in terms of computation time are Reynolds average Navier-Stokes (RaNS) equations which can be written as follows:

$$\frac{\partial U_i}{\partial t} + U_j \frac{\partial U_i}{\partial x_j} + \frac{\partial \overline{u_i u_j}}{\partial x_j} = -\frac{1}{\rho}\frac{\partial P}{\partial x_i} + \nu \frac{\partial^2 U_i}{\partial {x_j}^2}$$

Where $\overline{u_i u_j}$ represents the Reynolds stresses which must be modelled in order to close the system of equations. In this study Reynolds stresses are modelled using Spalart-Allamars (S-A) model and k-ω model.

BOUNDARY CONDITIONS

When considering three-dimensional internal fluid flow, four main boundary conditions can be considered, these are as follow:

Inlet boundary condition: Velocity magnitude normal to the boundary (4.44 m/s) and state of turbulence at the inlet represented by length scale and turbulent intensity.

Wall boundary condition: No-slip boundary condition with all velocity components equal zero at the wall.

Symmetry boundary condition: No flux across the symmetry boundary is imposed by setting the first derivatives of velocity components and turbulence quantities equal zero.

Outlet boundary condition: Mass flow weighting equals one.

COMPUTATIONAL MODEL

As the flow field is symmetric, only one quarter of the contraction and the test-section are considered. The computational geometry is meshed using Pointwise software. The mesh comprises of $1800 \times 150 \times 150$ grid points in x, y, and z, respectively. Since the turbulence models used in the present study demand low y^+ values for efficient resolution of viscous residuals, every effort was made to keep the y^+ value along the wall less than or equal 0.5.

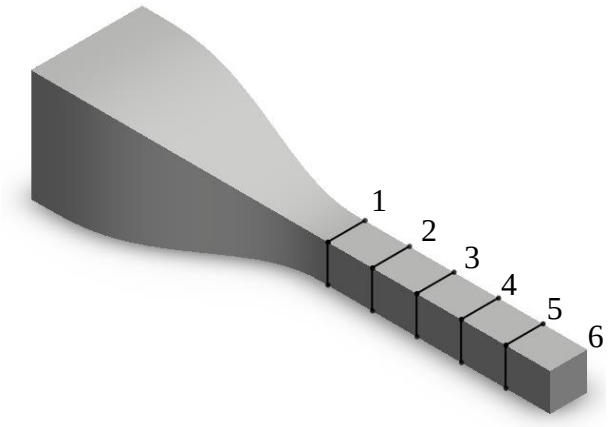

Figure 2 Sketch shows the computational domain

TURBULENCE MODELS

Both Spalart-Allmaras (S-A) and $k-\omega$ models are used for simulating the air flow behaviour in this study. Figure 3 shows that the two models give very close results, with a deviation of less than 0.15% for velocity differences. This in turn proves the low sensitivity of the results to turbulence models. All the following results are based on S-A model.

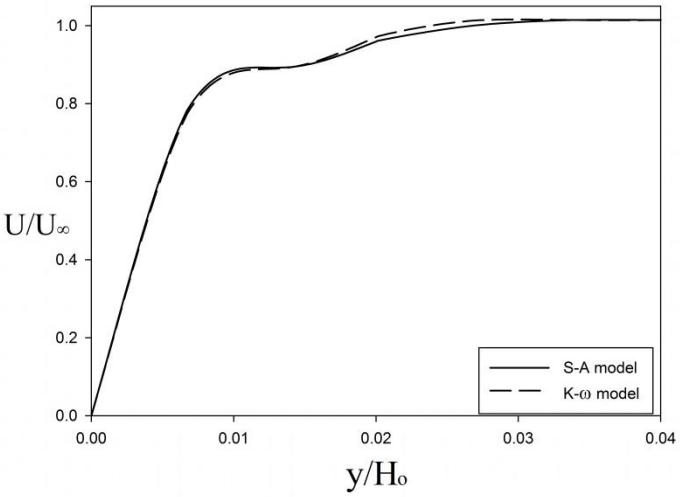

Figure 3 Stream-wise velocity profile at the test-section inlet for contraction profile three using S-A and k-ω models

BOUNDARY LAYER AND FLOW SEPARATION

At a solid surface the velocity of the fluid relative to the surface is zero which is known as the no-slip condition. This in turns, results in a region in which the velocity increases rapidly from zero at the surface to the main stream velocity known as the boundary layer region. Thus, high velocity gradients exist in the boundary layer region. The thickness of boundary layer is defined as the distance from the solid surface to the point at which the velocity reaches 99% of the free stream velocity. The thicker the boundary layer inside the test-sections of a wind-tunnel the narrower the domain at which an experiment can be performed. The flow separation typically occurs inside the boundary layer, when the reduction of velocity is combined with a positive pressure gradient known as an adverse pressure gradient opposing the main stream flow. The separation of the boundary layer causes a significant drop in the static pressure. In wind tunnel design, boundary layer separation in contraction must be avoided.

BOUNDARY LAYER THICKNESS

The results were analysed to test for the uniformity of the flow inside the test-section. The boundary layer profiles for the five contractions were plotted at five positions along the test-section to study the evolution of the boundary layer along the test- section. The five positions are shown in figure 2. Figures 4 to 8 illustrate that contraction number five has the thinner boundary layer, contractions four, three, two, and one follow respectively, with profile one having the thickest boundary layer. These results are suggesting that as the inflection point move further towards the contraction outlet the resulted boundary layer will be thinner, this is totally in agreement with the numerical results obtained by [5].

Figure 4 shows the five different boundary layer profiles at the test section inlet for the five contraction profiles. The variations between the boundary layer profiles tend to diminish as the probe moved towards the test section outlet. As shown in figure 9 the five boundary layer profiles tend to overlap at the test section outlet, indicating that the state of the flow become independent of the contraction profile as the air approaches downstream the test-section, i.e., the flow "forgets" which profile formed it in the contraction.

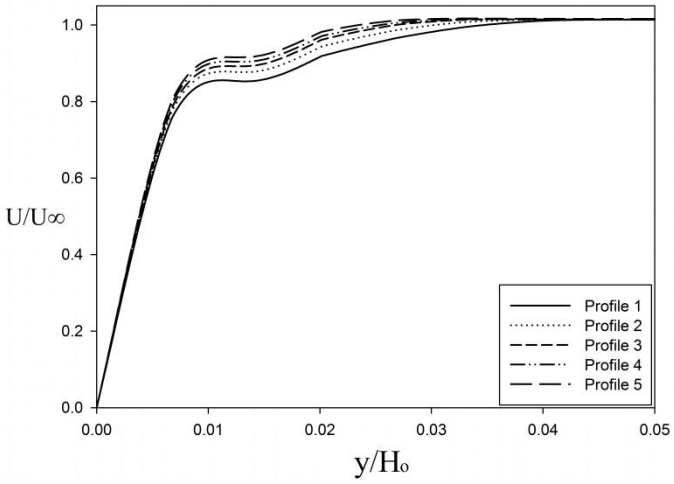

Figure 4 Boundary layer profiles at the test section inlet

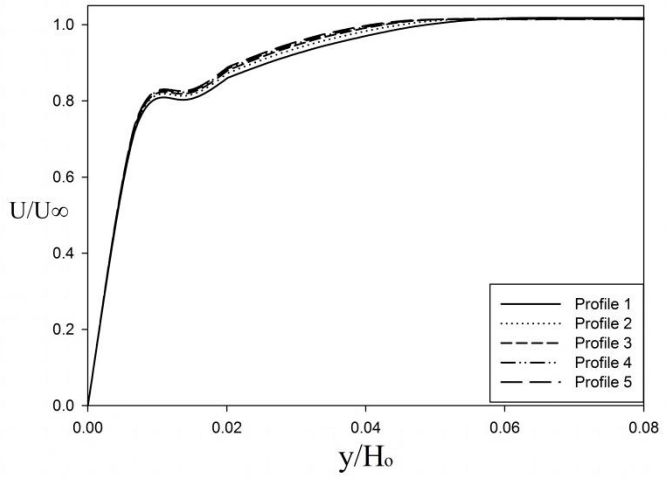

Figure 5 Boundary layer profiles at section 2

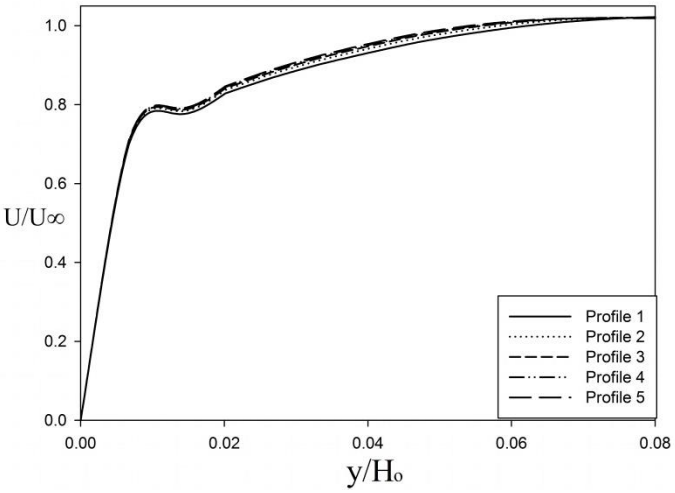

Figure 6 Boundary layer profiles at section 3

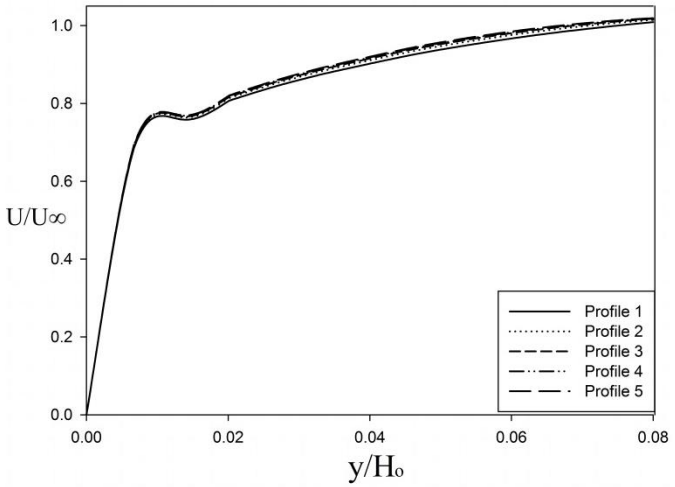

Figure 7 Boundary layer profiles at section 4

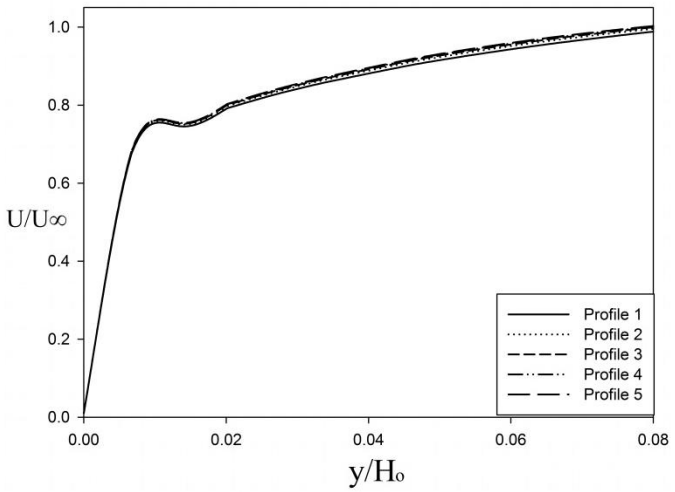

Figure 8 Boundary layer profiles at section 5

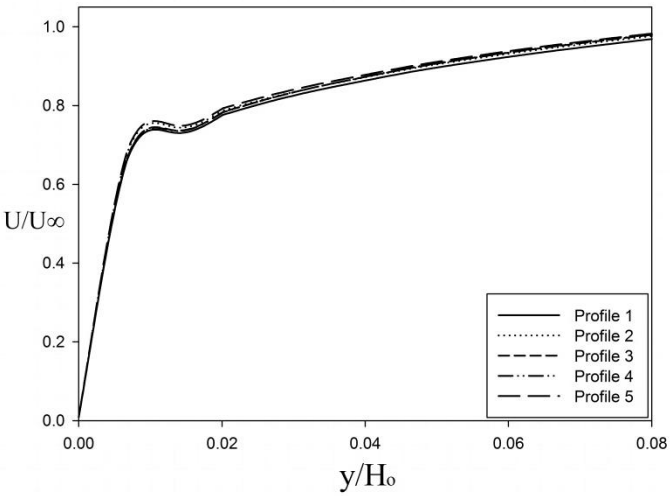

Figure 9 Boundary layer profiles at the test section outlet

STATIC PRESSURE

The pressure at the contraction inlet is assumed to be atmospheric pressure, as the settling chamber was not simulated in this case. The static pressure drops downstream as a result of area decrement, friction losses and local losses. Most of local losses are due to turbulence dissipation and flow separation. Vortices generated by flow separation are fed on the main stream energy. The maximum static pressure drop was detected close to the contraction outlet in all contraction profiles. This dramatic drop in static pressure indicates the location where the flow separation probability is the most. Contraction profile number five caused the maximum pressure drop, less pressure drop caused by contraction profile four, three, two and one respectively, as shown in figures 10 and 11.

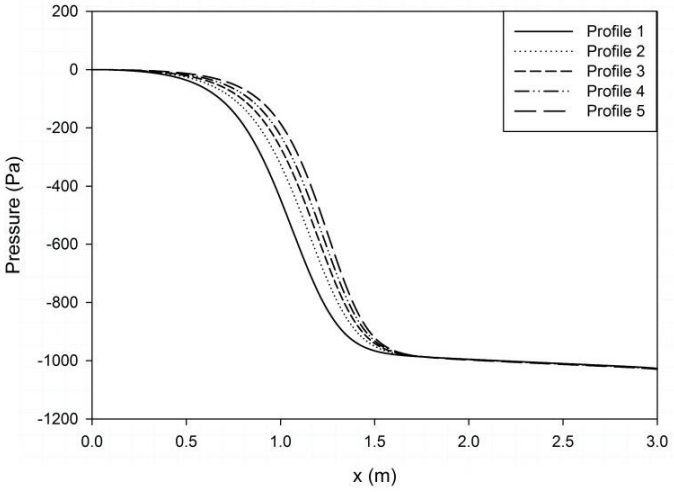

Figure 10 Static pressure for contraction profiles

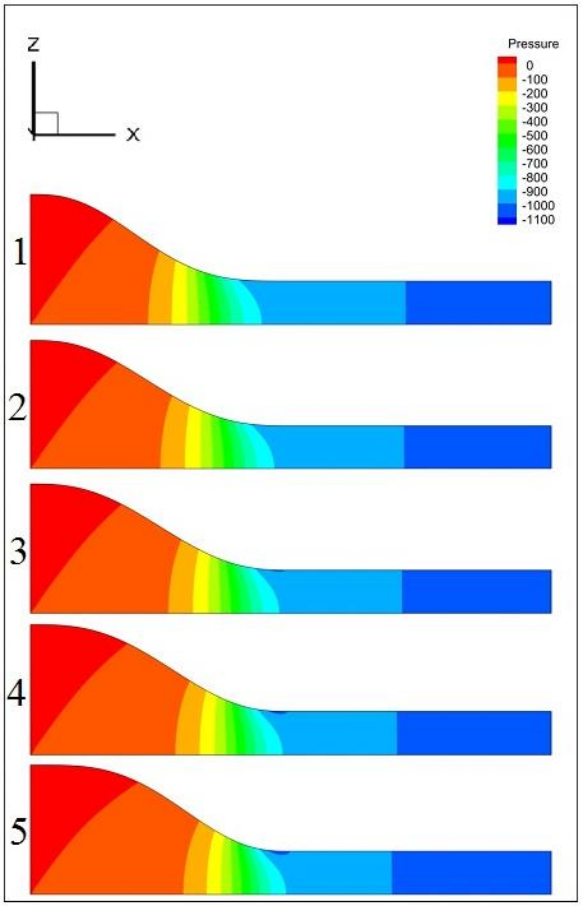

Figure 11 Static pressure contours

SECONDARY FLOW

The interaction between the vertical and horizontal boundary layers at the corners creates a region of secondary flow. In this region, significant variations in the wall normal velocity components, V and W velocities, are indicated at different sections along the test section by figures 12-15, the range of these variations are getting narrower as the boundary layers developed, i.e., the flow approaches the test section outlet to be in order of 0.7% of the mean flow velocity. The variation in V velocity was identical to that of W velocity. These boundary layers interactions generate two opposite vortices at each corner of the tunnel, as shown in figure 16, which have significant contributions to flow energy losses along the test section. The narrower range of variation in V and W velocities at the test section inlet achieved by contraction profile number one, then it increased for contraction profile number two, three, four, and five, respectively. Further downstream the test section the narrower range of variations was achieved by contraction profile five, and then it increased for contraction profile four, three, two, and one, respectively. Chamfer contraction corners are recommended for counteract the effect of secondary flow.

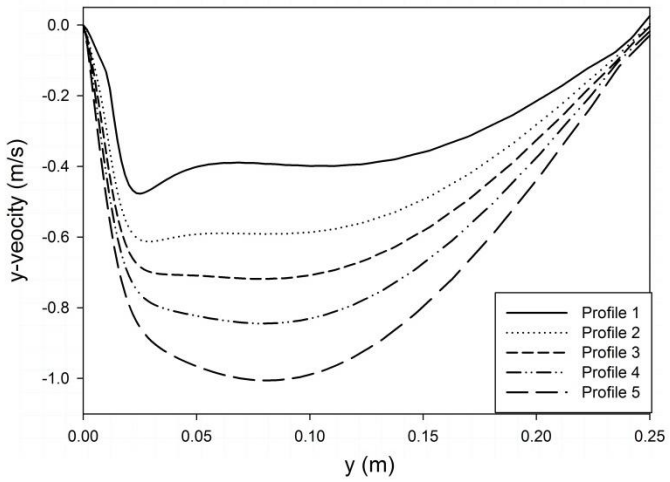

Figure 12 y-velocity in span wise direction at the test section inlet

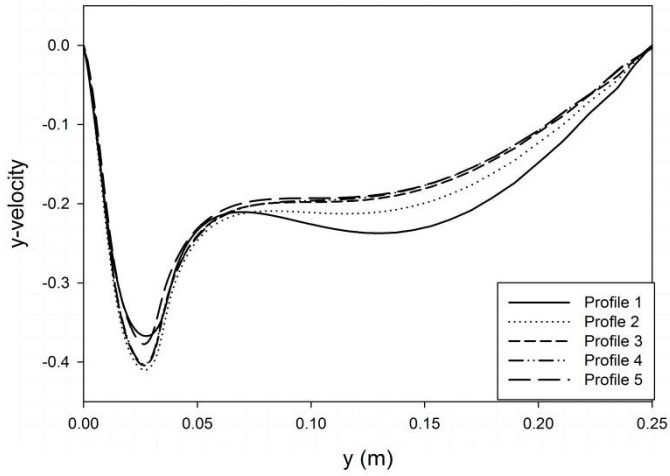

Figure 13 y-velocity in span wise direction at section 3 in the test section

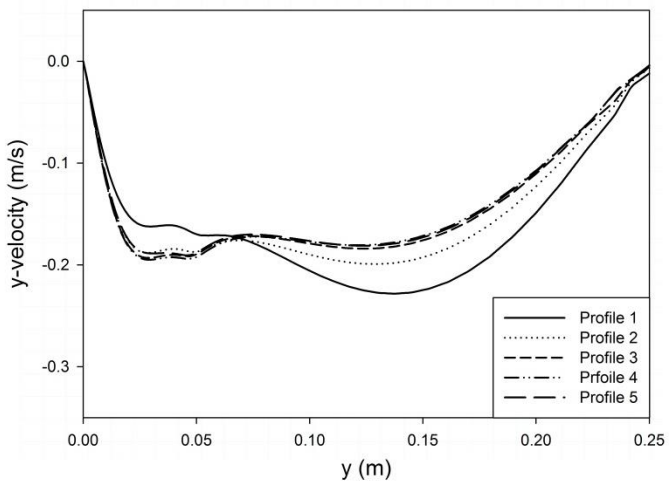

Figure 14 y-velocity in span wise direction at section 5 in the test section

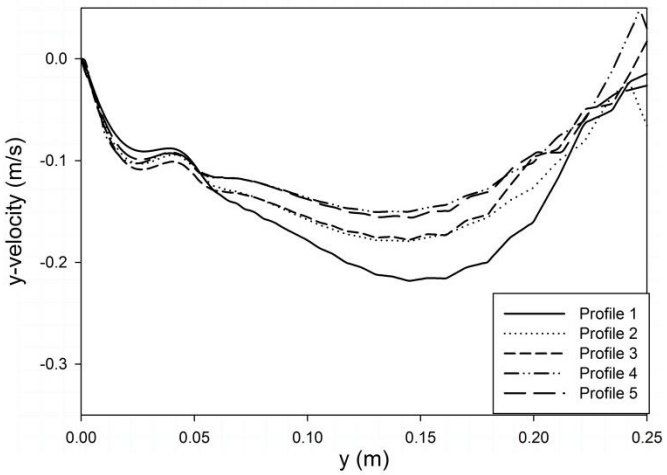

Figure 15 y-velocity in span wise direction at the test section outlet

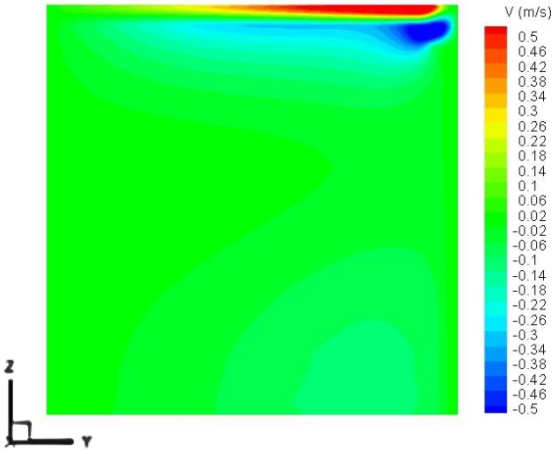

Figure 16 y-velocity at section 2

CONCLUSION

Computational fluid dynamics was used to analyse and optimize a three dimensional wind tunnel contraction. A six order polynomial equation was used to model the contraction profile. The location of the inflection point was the design parameter that varied along the contraction axis to give five different contraction profiles.

The numerical results indicated that the boundary layer thickness in the wind-tunnel test-section reduces as the inflection point moves downstream the contraction axis. The drop in static pressure decreases as the inflection point moves upstream the contraction axis. The variation in the wall normal velocities at the test section inlet reduces as the inflection point moves upstream, however, downstream the test section inlet these variations increases as the inflection point moves upstream. The following summary shows the best profile for each criterion:

- Boundary layer thickness: Profile five.
- Pressure drop: Profile one.
- Secondary flow: (Test-section inlet) Profile one.
- Secondary flow: (Downstream the test-section inlet) Profile five.

According to these criteria, as the inflection point is moved downstream, the first flow quality indicator gets better, the second flow quality indicator gets worse, and the third flow quality indicator depends on the position in the test section. Therefore, a compromise has to be made to balance the importance of each of the three flow quality indicators.

Based on these conclusions contraction profile number three, in which the inflection point is located at the middle of the contraction axis, was chosen to be the best profile for this wind-tunnel. The chosen contraction profile is a fifth order polynomial since the inflection point was located at the middle of the contraction for this profile.

REFERENCES

[1] Morel, T., Comprehensive Design of Axisymmetric Wind TunnelContractions, *ASME Journal of Fluids Engineering*, 1975, *pp.225-233.*

[2] Mehta R. D. and Bradshaw P., Design Rules for Small Low SpeedWind-Tunnels, *Aeronautical Journal Nov. 1979, No. 718, PP. 443-449.*

[3] Ramaseshan, S. and Ramaswamy, M.A., A Rational Method to Choose Optimum Design for Two-Dimensional Contractions, *ASME Journal of Fluids Engineering, No. 124,* 2002, *pp. 544-546.*

[4] Johl M., Passmore M. and Render P., Design Methodology andPerformance of an Iindraft Wind-Tunnel, *The Aeronautical Journal*,2004, pp. 465-473.

[5] Sargison J. E., Walker G. J., and Rossi R., Design and calibrationof a wind tunnel with a two dimensional contraction, *15th Australasian Fluid Mechanics Conference,* 2004.

[6] Winkler J., Temel F., and Carolus T., Concept, Design and Characterization of A Small Aero-acoustic Wind Tunnel Facility With Application To Fan Blade Measurements, *Fan Noise, Lyon- France, 17-19 September 2007.*

[7] Yao-xi Su, Flow Analysis and Design of Three Dimensional Wind Tunnel Contractions, AIAA, Vol. 29, No.11.

[8] Lindgren B. and Johansson A. V., Design and Evaluation of a Low-Speed Wind-Tunnel with Expanding Corners, M.Sc. thesis, Department of Mechanics, KTH, Sweden.

[9] Mikhail, M. N. & Rainbird, W. J., Optimum design of wind tunnel contractions, *paper 78-819. In AIAA 10th Aerodynamic Testing Conference.*